

SCAR: State-Space Compression for Scalable AI-Based Network Management of Vehicular Services

Ioan-Sorin Comşa, Purav Shah, Karthik Vaidhyanathan, Deepak Gangadharan, Christof Imhof, Per Bergamin, Aryan Kaushik, Gabriel-Miro Muntean, and Ramona Trestian

Abstract—The increasing demand for connected vehicular services poses significant challenges for AI-based network and service management due to the high volume and rapid variability of network state information. Traditional management and control mechanisms struggle to scale when processing fine-grained metrics such as Channel Quality Indicators (CQIs) in dynamic vehicular environments. To address this challenge, we propose SCAR (State-Space Compression for AI-Based Network Management), an edge-assisted framework that improves scalability and fairness in vehicular services through network state abstraction. SCAR employs machine-learning (ML)-based compression techniques, including clustering and radial basis function (RBF) networks, to reduce the dimensionality of CQI-derived state information while preserving essential features relevant to management decisions. The resulting compressed states are used to train reinforcement learning (RL)-based management policies that aim to maximize network efficiency while satisfying service-level fairness objectives defined by the NGMN. Simulation results show that SCAR increases the time spent in feasible management regions by 14% and reduces unfair service allocation time by 15% compared to reinforcement learning baselines operating on uncompressed state information. Furthermore, simulated annealing with stochastic tunneling (SAST)-based clustering reduces state compression distortion by 10%, confirming the effectiveness of the proposed approach. These results demonstrate that SCAR enables scalable and fair AI-assisted network and service management in dynamic vehicular systems.

Index Terms—Vehicular Services, Network and Service Management, AI-Assisted Network Control, State-Space Compression, Reinforcement Learning.

I. INTRODUCTION

The evolution of mobile networks toward increasingly intelligent and software-driven architectures has significantly expanded the scope of network and service management, enabling support for data-intensive and latency-sensitive applications [1]. While much of the recent research has focused on mission-critical Ultra-Reliable Low-Latency Communication

(URLLC) services [2], there is an equally pressing demand for high-throughput and delay-sensitive vehicular services such as infotainment, cloud gaming, augmented reality (AR), and high-definition video streaming [3]. Supporting these services requires not only seamless connectivity but also scalable and adaptive network management mechanisms capable of operating under highly dynamic vehicular conditions.

Autonomous and connected vehicles continuously generate large volumes of heterogeneous data, including sensor information and fine-grained network state measurements such as Channel Quality Indicators (CQI), Signal-to-Noise Ratio (SNR), and latency metrics. Efficient processing of such state information is essential for maintaining service quality and fairness. However, relying on uncompressed CQI reports introduces substantial computational overhead, increases control-plane load, and limits the responsiveness of real-time network management and scheduling functions [4]. These challenges are further exacerbated by mobility-induced variability in Vehicular Edge Computing (VEC) systems, which affects computation offloading decisions and service-level resource management performance [5]. Prior studies have emphasized the importance of adaptive, edge-based optimization strategies in mobile environments, including UAV-assisted and wireless-powered MEC systems [6], [7], as well as the role of edge intelligence in improving resource efficiency for vehicular services [8].

Conventional resource management mechanisms, often based on centralized control logic and predefined heuristics, are not well-suited to the rapid state fluctuations and high data demands of vehicular networks [9]. Machine Learning (ML) has emerged as a promising paradigm for addressing these complexities, enabling data-driven decision-making across tasks such as interference management, link adaptation, beam selection, and resource management [10]. Reinforcement learning (RL), in particular, has demonstrated the ability to learn adaptive control policies from historical observations [11]. Yet, these approaches often struggle to scale in real-time scenarios due to the high dimensionality of raw CQI data and the computational cost of training on large state spaces.

To address these challenges, we propose SCAR (State-Space Compression for AI-Based Network Management), an edge-assisted framework that enables scalable and adaptive management of vehicular services through network state abstraction. SCAR transforms high-dimensional CQI reports into compact, informative representations through a two-stage pipeline,

I.-S. Comşa, C. Imhof, and P. Bergamin are with the Institute for Research in Open-, Distance- and eLearning, Swiss Distance University of Applied Sciences, Brig, CH-3900, Switzerland (e-mails: {ioan-sorin.comsa, christof.imhof, per.bergamin}@ffhs.ch). P. Shah and R. Trestian are with London Digital Twin Research Centre, Middlesex University London, NW4 4BT, Hendon, London, U.K. (e-mails: {r.trestian, p.shah}@mdx.ac.uk). K. Vaidhyanathan is with the Software Engineering Research Center, IIT-Hyderabad, Hyderabad 500032, India. (e-mail: karthik.vaidhyanathan@iit.ac.in). D. Gangadharan is with the Computer Systems Group, IIT Hyderabad, Hyderabad 500032, India. (e-mail: deepak.g@iit.ac.in). A. Kaushik is with the Department of Computing and Mathematics, Manchester Metropolitan University, U.K., e-mail: (a.kaushik@mmu.ac.uk). G.-M. Muntean is with School of Electronic Engineering, Dublin City University, D09 V209, Dublin, Ireland (e-mail: gabriel.muntean@dcu.ie).

where offline K-means clustering defines CQI pattern groups used by online RBFN classification to efficiently recognize new CQI reports in real time. These compressed states feed into a RL-based management controller, enabling efficient and fair resource allocation aligned with NGMN-defined objectives. By embedding compression-aware intelligence at the edge, SCAR addresses key challenges of scalability, latency, and fairness, enabling effective AI-assisted network and service management for dynamic vehicular services.

A. Related Work

Efficient classification and abstraction of network state information are essential for scalable ML-driven network and service management, particularly in highly dynamic vehicular environments. K-means clustering, a widely used unsupervised learning method, is valued for its simplicity and effectiveness in minimizing intra-cluster distances [12]. It has been applied in various wireless domains, including mmWave multipath partitioning [13], cooperative spectrum sensing [14], user behavior analysis [15], and content caching strategies [16]. However, these applications typically assume static or slowly varying data distributions and lack the real-time adaptability required in vehicular networks. SCAR addresses this gap by embedding K-means into a CQI compression pipeline optimized for edge-based learning under rapid state changes. While known limitations of K-means, such as sensitivity to initialization and convergence to local optima, have been mitigated through techniques including randomized restarts and improved seeding strategies [17], the use of K-means for real-time network state abstraction in vehicular network management remains largely unexplored.

When labeled data is available, supervised learning techniques are commonly employed for classification and prediction tasks in network management and control [18]. Methods such as k-nearest neighbors, decision trees, Bayesian classifiers, and support vector machines have all been applied to RRM scenarios [19]. Neural networks have also been used to predict cellular traffic patterns [20] and estimate QoS indicators based on varying loads [21]. Hybrid models that combine unsupervised clustering with supervised learning (e.g., using K-means to pre-structure data before classification) have improved the content dissemination and interference management [22], [23]. However, these frameworks are often not optimized for low-latency environments. In this context, RBFN presents a promising alternative due to their fast inference capabilities and compatibility with clustering-based inputs [24]. Notably, SCAR is among the first frameworks to leverage RBFNs for network state classification derived from CQI measurements, combining offline clustering with online, low-latency classification to support real-time management decisions in vehicular environments.

Reinforcement learning has attracted significant attention for adaptive network and service management, as it enables controllers to learn decision-making policies through continuous interaction with the environment rather than relying solely on static models or labeled datasets [18]. This makes RL particularly suited to highly dynamic vehicular environments, where rapid adaptation to changing network conditions is

essential. However, RL-based management controllers in such settings face significant challenges due to high-dimensional, multi-agent state spaces, which require effective dimensionality reduction to remain scalable and efficient [25]. One notable example is the Cluster-enabled Cooperative Scheduling based on Reinforcement Learning (CCSRL) [26], which improves V2V communication reliability using cluster-based task scheduling and RL-assisted auxiliary transmission scheme in dynamic vehicular networks. While effective, CCSRL assumes access to fine-grained state information and does not address the impact of state dimensionality on learning efficiency. In contrast, SCAR directly targets this limitation by compressing CQI-derived network state representations and structuring them to enable scalable, low-latency RL-based network management.

The need for compression-aware learning and control is further amplified by the growing demand for data-intensive vehicular services. Applications such as cloud gaming, high-definition video streaming, and augmented reality require not only high throughput but also consistent low-latency service allocation to maintain user experience. In this context, Multi-access Edge Computing (MEC) has become essential for enabling real-time processing close to the vehicle, reducing response times and improving QoS [27]. Additionally, cooperative data sharing and edge-assisted perception in autonomous systems have highlighted the value of intelligent compression and distributed learning mechanisms [28]. These insights extend naturally to vehicular services, where large volumes of network state information must be processed rapidly to adapt to changing conditions. SCAR's edge-assisted state compression framework directly addresses these requirements by reducing state dimensionality and enabling efficient learning-based management.

Several CQI and state compression techniques have been proposed primarily to reduce signaling overhead rather than to address scalability challenges in learning-based network management. Feedback-based schemes transmit CQI only when user scheduling probabilities exceed certain thresholds [29], while K-means-based methods aim to lower congestion through pattern clustering [30], and deep learning models have been applied in massive MIMO systems [31]. However, these approaches generally do not tackle the core issue of CQI dimensionality reduction required for efficient RL training. Some efforts, such as average CQI representations for wide-band scheduling [32], offer partial solutions but lack general applicability. In contrast, SCAR introduces a unified state-space compression framework that combines clustering-based feature extraction with RBFN classification to enable scalable, low-latency reinforcement learning-based network and service management in vehicular environments.

B. Contributions

This paper proposes SCAR (State-Space Compression for AI-Based Network Management), a framework designed to enable scalable and fair AI-assisted network and service management for dynamic vehicular services. By abstracting high-dimensional CQI-derived network state information at the network edge, SCAR facilitates efficient learning-based

control under rapidly changing vehicular conditions. The main contributions of this work are summarized as follows:

1) *State-Space Compression via Offline Clustering Optimization*: We introduce a Simulated Annealing with Stochastic Tunneling (SAST)-enhanced K-means clustering method to construct representative network state prototypes from large-scale CQI datasets. The proposed optimization improves cluster quality by mitigating sensitivity to initialization and reducing convergence to local optima, enabling robust state abstraction for downstream learning tasks.

2) *Low-Latency Online State Classification at the Edge*: An online radial basis function network (RBFN) classifier is integrated to enable real-time classification of incoming CQI-derived state information based on the precomputed clusters. The lightweight inference and generalization capability of the RBFN support low-latency state recognition, making the framework suitable for edge-assisted network management in highly dynamic vehicular environments.

3) *Compression-Aware Reinforcement Learning for Network Management*: The compressed network state representations are leveraged by a RL-based management controller to guide service allocation decisions under fairness constraints. By operating on the reduced state space, the proposed approach improves learning efficiency and scalability, achieving over 15% improvement in service-level fairness while reducing computational overhead compared to RL approaches using uncompressed state information.

4) *Scalability and Generality of the Management Framework*: SCAR is designed as a technology-agnostic state abstraction and management framework that can be integrated with different access technologies and resource control mechanisms across network domains. This generality allows the proposed approach to support diverse vehicular service scenarios without requiring assumptions about specific radio access schemes.

C. Paper Organization

The rest of the paper is organized as follows: Section II presents the proposed SCAR framework and the RL-based management model. In Section III, the proposed CQI compression scheme based on K-means algorithm and RBFN classification is detailed. Section IV analyzes the simulation results for the SCAR framework and shows the advantage of using the proposed compression framework in RL-based management systems. Finally, Section V concludes the paper.

II. PROPOSED SCAR FRAMEWORK

The SCAR framework, illustrated in Fig. 1, is designed to support scalable and adaptive AI-assisted network and service management for dynamic vehicular environments. As connected vehicles increasingly rely on bandwidth-intensive applications (e.g. cloud gaming, HD video streaming, and AR-based entertainment), network controllers must operate over rapidly changing and high-dimensional state information. SCAR addresses this challenge by introducing a compression-aware management architecture that enables learning-based control to scale efficiently under vehicular mobility. SCAR integrates three tightly coupled components: (1) edge-assisted CQI compression, (2) RL-based management policy control,

and (3) distributed model refinement across edge and cloud domains. By performing state abstraction close to the network edge, SCAR significantly reduces signaling overhead and computational latency, allowing management decisions to be made in near real time.

To handle the large volume of fine-grained network state information generated by vehicular users, SCAR employs a two-stage ML pipeline at the network edge. First, a K-means clustering algorithm, enhanced with SAST algorithm, groups similar CQI conditions into representative clusters, effectively reducing state-space dimensionality. Second, the RBF network classifies incoming CQI reports based on these clusters, enabling fast and robust state recognition with minimal computational overhead. This compressed yet informative representation of network conditions ensures that RL-based management policies can operate on a fixed-dimensional state space, even as the number of active users and channel conditions fluctuate rapidly.

Once CQI data is compressed at the edge, it is transmitted to a RL-based management controller that dynamically adjusts resource allocation parameters based on observed system conditions and service-level objectives, with a particular focus on fairness as defined by NGMN guidelines. By operating on compressed state representations rather than raw CQI vectors, the management controller improves learning efficiency, reduces convergence time, and maintains stable performance under high mobility and dense user populations. This enables SCAR to support consistent service quality while adapting to rapidly changing vehicular environments.

To enhance long-term adaptability, SCAR incorporates a distributed learning architecture in which compressed state information and management feedback from multiple edge nodes are periodically aggregated. This aggregated knowledge is used to refine global management models, capturing broader operational trends and vehicular behavior patterns across diverse environments.

Updated models and parameters are subsequently redistributed to edge nodes, enabling continuous improvement of state compression and management policies without requiring centralized real-time control. This design supports scalability while preserving the low-latency operation required for vehicular services.

A. RL-Based Management Model

The RL-based management system, illustrated in Fig. 2, consists of three functional components: a resource allocation mechanism, an intelligent management controller, and a state compression module. At each transmission time interval (TTI), resources are allocated across active users while ensuring that service-level fairness constraints are respected. The intelligent management controller dynamically adjusts control parameters based on the current network state (CQI reports, user throughput, user count, etc.) to optimize fairness, including compressed CQI information, user throughput statistics, and system load. Due to the continuous and high-dimensional nature of the control problem, reinforcement learning is employed to approximate optimal management policies. This

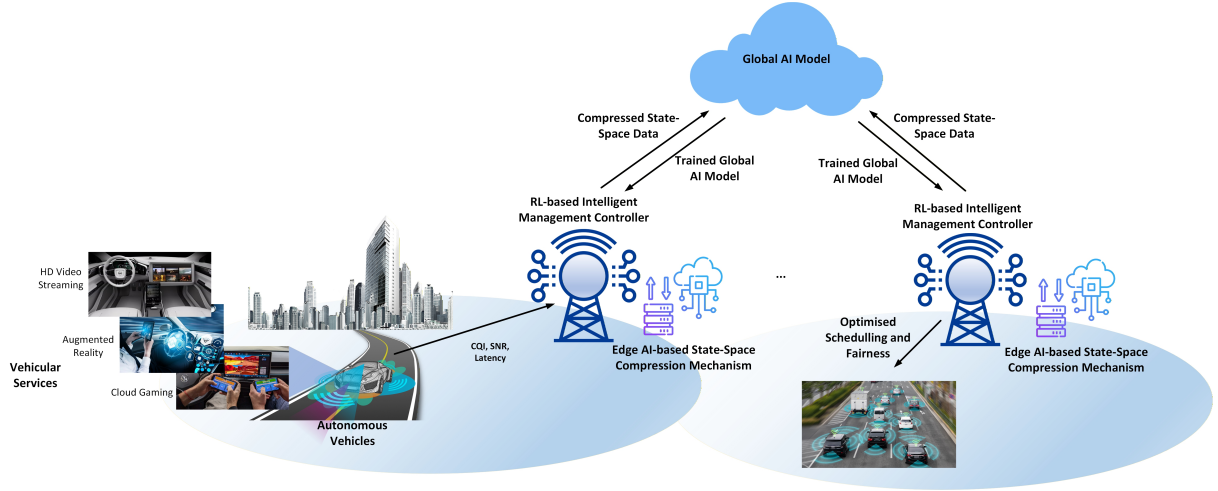


Fig. 1: Proposed SCAR Framework

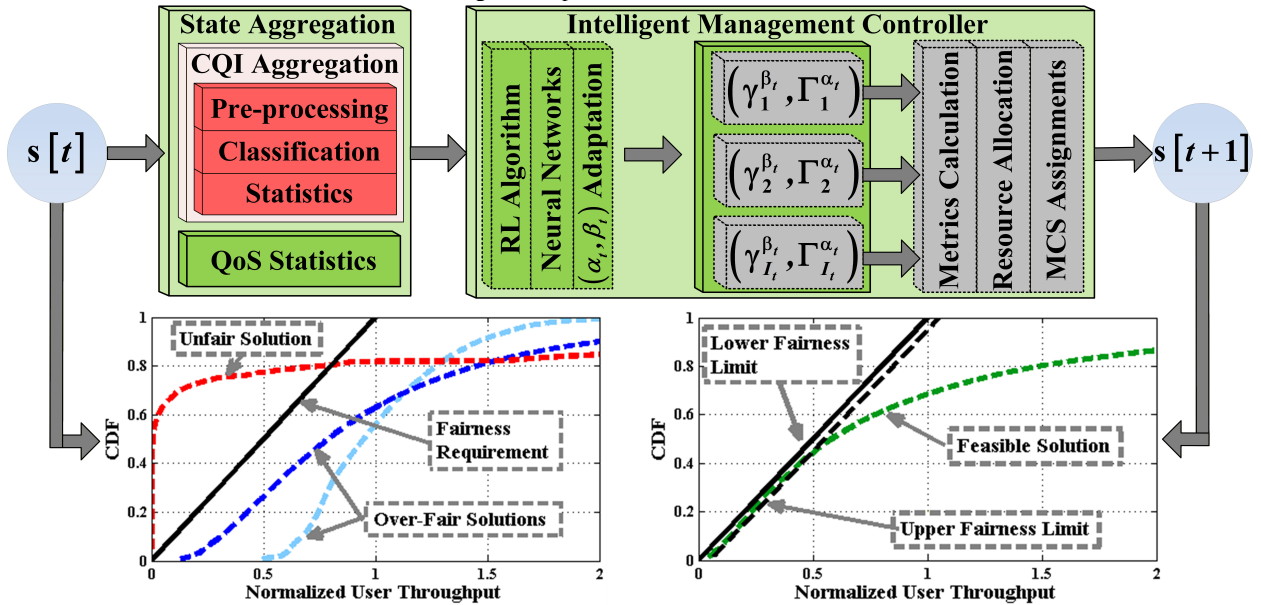


Fig. 2: RL-Based Management System.

work evaluates a range of RL algorithms [11], including Q-Learning, Double-Q, SARSA, Actor-Critic, and QV variants, trained using compressed CQI network state representations. The objective is to maximize overall network efficiency while ensuring that service-level fairness constraints, as defined by NGMN, remain satisfied over time.

The intelligent management controller's state is inherently variable in dimension, as it depends on the number of active users, which fluctuates over time. To manage this variability and reduce state complexity, a compression mechanism is required. While basic QoS indicators can be summarized using statistical measures (e.g., mean, standard deviation), CQI reports are more complex, as they form bandwidth-dependent vectors whose number scales with both system bandwidth and user count. To address this, this paper proposes a novel CQI compression mechanism that effectively extracts meaningful patterns from high-dimensional CQI data, enabling consistent and scalable state representation for RL-based management system.

1) *Fairness-Oriented Control*: We define $\mathcal{I}_t = \{1, 2, \dots, I_t\}$ as the set of active User Equipments (UEs)

at TTI t , where I_t denotes the number of users. Each user $i \in \mathcal{I}_t$ generates traffic to be managed under fairness constraints. The total system bandwidth is divided into J Resource Blocks (RBs), represented by $\mathcal{J} = \{1, 2, \dots, J\}$. Let $\mathbf{\Gamma}[t] = [\Gamma_1, \Gamma_2, \dots, \Gamma_{I_t}]$ denote the vector of average user throughputs at time t , where Γ_i is the throughput of user i . The management controller assigns RBs from \mathcal{J} to users in \mathcal{I}_t with the objective of maximizing system throughput while maintaining fairness based on the NGMN criterion [33], which requires the CDF of $\Gamma_i[t]$ to lie to the right of a predefined reference line (see Fig. 2). Due to dynamic network conditions, the management controller must be updated at each TTI to adhere to this fairness constraint by solving the following problem:

$$\begin{aligned} & \max_a \sum_i \sum_j a_{i,j}[t] \cdot \frac{[\gamma(x_{i,j})]^{\beta_t}}{\Gamma_i^{\alpha_t}}, \\ & s.t. \end{aligned} \quad (1)$$

$$\sum_i a_{i,j}[t] \leq 1, \quad j = 1, 2, \dots, J, \quad (1.a)$$

$$a_{i,j}[t] \in \{0, 1\}, \quad \forall i \in \mathcal{I}_t, \forall j \in \mathcal{J}, \quad (1.b)$$

$$\Upsilon_i(\Gamma_i, \mathbf{\Gamma}) \leq \Upsilon_i^R, \quad i = 1, 2, \dots, I_t. \quad (1.c)$$

The optimization problem in (1) models the RB allocation process, where $a_{i,j} \in \{0, 1\}$ is a binary decision variable indicating whether RB $j \in \mathcal{J}$ is assigned to UE $i \in \mathcal{I}_t$. The achievable rate $\gamma_{i,j}$ depends on the CQI value $x_{i,j} \in \{1, 2, \dots, N\}$, which determines the maximum number of bits $\delta_{i,j}$ transmittable on RB j for user i . This is mapped via a predefined function $\gamma(x_{i,j})$, where $\gamma_{i,j}[t] = \delta_{i,j}/0.001$. The optimization objective is controlled by parameters $\{\alpha_t, \beta_t\} \in [-1, 1]$, which balance system throughput and fairness:

- If $\beta_t > \alpha_t$, the management controller favors users with higher CQI values to maximize throughput.
- If $\alpha_t \geq \beta_t$, it prioritizes users with lower average throughput to promote fairness.

Constraints (1.a) ensure each RB is assigned to at most one user, while constraints (1.b) reflect the combinatorial nature of the allocation. Constraints (1.c) enforce the NGMN fairness criterion, where $\Upsilon_i(\Gamma_i, \mathbf{\Gamma})$ is the normalized CDF of user i 's throughput, and Υ_i^R is the required minimum value defined by the reference line shown in Fig. 2.

The solution to (1) aims to allocate each RB $j \in \mathcal{J}$ to the user $i \in \mathcal{I}_t$ that maximizes the ratio $[\gamma(x_{i,j})]^{\beta_t}/\Gamma_i^{\alpha_t}$, while satisfying the NGMN fairness constraint in (1.c). However, due to varying channel conditions and user mobility, fixed parameter settings α_t and β_t may lead to suboptimal outcomes, either unfair resource allocation (when $\beta_t > \alpha_t$) or overly fair allocations that degrade system throughput (when $\alpha_t > \beta_t$), as illustrated in Fig. 2. To address this, the intelligent management controller must dynamically learn the optimal parameterization $[\alpha_t, \beta_t]$ at each TTI to keep the throughput CDF Υ_i as close as possible to the NGMN requirement line Υ_i^R , while staying above a defined lower threshold Υ_i^L . A solution is considered feasible when it satisfies the condition:

$$\Upsilon_i^L \leq \Upsilon_i \leq \Upsilon_i^R. \quad (2)$$

The intelligent management controller's role is to adjust these parameters in real time to maintain the solution within this feasibility region and ensure long-term fairness-compliant services.

2) *Fairness Adaptation Mechanism:* The fairness adaptation mechanism aims to maximize the time the intelligent management controller operates within the feasible region defined by the NGMN fairness criterion, while minimizing periods of unfair resource allocation. This is achieved through a RL process, where the intelligent controller learns to associate each controller state $\mathbf{s}[t] \in \mathcal{S}$ with the optimal fairness parameters $[\alpha_t, \beta_t]$. At each TTI t , the controller observes the state, selects an action by updating $[\alpha_t, \beta_t]$, and receives a reward at $t + 1$ based on how well the resulting throughput CDF satisfies the fairness constraint. Neural networks are used to approximate the optimal parameterization due to the continuous and multidimensional nature of the state space. The initial state vector is defined as:

$$\mathbf{s} = [\alpha_{t-1}, \beta_{t-1}, \mathbf{\Gamma}, \mathbf{x}, I_t], \quad (3)$$

where $\mathbf{x} = [\mathbf{x}_1, \dots, \mathbf{x}_{I_t}]$ represents the CQI vectors of all users and $\mathbf{x}_i = [x_{i,1}, \dots, x_{i,J}]$ corresponds to the CQI values for user i . Due to the variability in user count I_t and bandwidth-dependent CQI reports, the state dimension changes over time. To enable efficient learning, SCAR introduces a state compression mechanism that reduces \mathbf{s} to a fixed dimension. While user throughput $\Gamma[t]$ is modeled as a log-normal distribution and compressed using mean and standard deviation [11], CQI compression is more complex. SCAR employs a learning-based CQI compression technique to extract relevant features from high-dimensional input, enabling the controller to make informed parameterization decisions and steer the intelligent controller toward fairness-compliant operation within the feasible region.

B. SAST-Based Optimization

To enhance the performance of the SCAR framework in both CQI clustering and classification, we adopt an optimization technique based on Simulated Annealing with Stochastic Tunneling (SAST). This meta-heuristic method is well-suited for exploring large, non-convex search spaces and finding globally optimal solutions under uncertainty. In the context of SCAR, the SAST algorithm is applied to two key problems: (i) the selection of optimal CQI cluster centers during offline K-means clustering, and (ii) the tuning of RBFN weights in the online classification phase.

Let \mathcal{B} denote the current state (e.g., a set of CQI cluster centers or RBFN weights), and \mathcal{A} a candidate neighboring solution. The acceptance probability of transitioning from \mathcal{B} to \mathcal{A} is defined as [34]:

$$\mathbb{P}(\mathcal{A}|\mathcal{B}) = \min [1, \mathbb{F}(\mathcal{A}, \mathcal{B}, \mathbf{T})], \quad (4)$$

where \mathbf{T} is a global temperature parameter, and $\mathbb{F}(\cdot)$ is the acceptance function, defined as [34]:

$$\mathbb{F}(\mathcal{A}, \mathcal{B}) = \exp \left[-\frac{F(\mathcal{A}) - F(\mathcal{B})}{\mathbf{T}} \right], \quad (5)$$

with $F(\cdot)$ being the stochastic tunneling function that normalizes the energy relative to the best solution found so far [34]:

$$F(\mathcal{X}) = 1 - \exp \left[-\frac{f(\mathcal{X}) - f^*}{\omega} \right], \quad (6)$$

where $\mathcal{X} \in \{\mathcal{A}, \mathcal{B}\}$, $f(\mathcal{X})$ is the energy (cost) of state \mathcal{X} , f^* is the minimum energy observed so far, and ω is the tunneling parameter. In the CQI clustering problem, $f(\mathcal{X})$ represents the Euclidian distance between CQI centers and other CQI points, while in RBFN training, it may denote the classification loss. The SAST mechanism enables escape from local minima by comparing energy values against f^* and accepting worse states with a probability that decreases as the temperature \mathbf{T} lowers. The initial temperature is computed as [34]:

$$\mathbf{T}_0 = -\sum_{l=1}^L [F_l(\mathcal{A}) - F_l(\mathcal{B})] / [L \cdot \ln(\mathbb{P}_0)], \quad (7)$$

where L is the number of sampling iterations and \mathbb{P}_0 is the initial acceptance probability. The temperature is then gradually reduced at each iteration based on:

$$\mathbf{T}_{new} = \mathbf{T}_{old} \cdot R_T, \quad (8)$$

where $R_T \in [0, 1]$ is the cooling rate.

By applying SAST in both the offline clustering and online classification stages, SCAR enhances its ability to gener-

ate robust CQI representations and maintain accurate, low-latency state classification. This significantly improves the performance of the subsequent RL-based resource allocation, ensuring that fairness and throughput objectives are better met under real-time vehicular dynamics.

III. PROPOSED CQI COMPRESSION MECHANISM

As shown in Fig. 2, the proposed CQI compression mechanism operates in three stages. First, a pre-processing stage removes system bandwidth dependency from CQI reports. Next, the classification stage uses a two-step learning approach: K-means clustering (unsupervised) identifies structural patterns in CQI data, while a RBF network (supervised) classifies new CQI inputs into these learned clusters. Finally, the statistical stage extracts key features from the classified CQI space to support low-latency, edge-assisted operation.

A. Preprocessing Stage

The preprocessing stage transforms each CQI report $\mathbf{x}_i = [x_{i,1}, \dots, x_{i,J}]$ from bandwidth-dependent vectors into normalized histograms independent of system bandwidth. This is done by computing the frequency distribution of CQI values:

$$\mathbf{y}_i = [y_{i,1}, y_{i,2}, \dots, y_{i,N}], \quad (9)$$

where $y_{i,n}$ is the normalized count of CQI value n for user i :

$$y_{i,n} = \frac{1}{J \cdot n} \sum_{\substack{j=1 \\ x_{i,j}=n}}^J x_{i,j}, \forall i \in \mathcal{I}_t, n = \{1, \dots, N\}, \quad (10.a)$$

$$\sum_{n=1}^N y_{i,n} = 1, \forall i \in \mathcal{I}_t. \quad (10.b)$$

Although this reduces dimensionality from J to N , many values in \mathbf{y}_i remain insignificant. To further reduce complexity, the top- M most significant entries are selected:

$$\mathcal{M}_i = \{y_{i,n,1}, \dots, y_{i,n,M}\}, \quad (11.a)$$

$$\mathcal{R}_i = \{y_{i,n,M+1}, \dots, y_{i,n,N}\}, \quad (11.b)$$

where the elements in \mathbf{y}_i are sorted in descending order:

$$y_{i,n,1} > y_{i,n,2} > \dots > y_{i,n,N}. \quad (12)$$

Residual values \mathcal{R}_i are redistributed to the nearest top- M values from \mathcal{M}_i to preserve normalization:

$$y_{i,n,p} = \begin{cases} y_{i,n,m} + \sum_{r_m}^{R_m} y_{i,n,r_m}, & m \leq M \\ 0, & \text{otherwise.} \end{cases} \quad (13)$$

resulting in a bandwidth-independent preprocessed vector:

$$\mathbf{y}_{i,M} = [y_{i,n,1}, y_{i,n,2}, \dots, y_{i,n,M}, 0, \dots, 0], \quad (14)$$

with elements reordered according to the original CQI index n . These compact vectors are then used in the classification stage to group similar CQI patterns. A two-step learning process is applied: *a*) unsupervised learning (K-means) identifies K representative CQI patterns; and *b*) supervised learning (RBFN) classifies each $\mathbf{y}_{i,M}$ to one of the K classes. This yields a classification vector at each TTI:

$$\mathbf{v}_M[t] = [v_{M,1}, v_{M,2}, \dots, v_{M,K}], \quad (15)$$

where $v_{M,k}$ denotes the number of users whose CQI patterns belong to class k . The joint parameterization of $\{M, K\}$ is critical for balancing compression accuracy and resource management efficiency in AI-assisted vehicular services.

B. Unsupervised Machine Learning

In SCAR, unsupervised learning is used to identify representative clusters from pre-processed CQI data. Let $\mathcal{U}_M = \{\mathbf{y}_{u,M} \mid u = 1, 2, \dots, U_M\}$ be the set of U_M distinct top- M pre-processed CQI vectors. The goal is to compute a set of K_M cluster centers $\mathcal{K}_M = \{\mathbf{c}_k \mid k = 1, 2, \dots, K_M\}$, where each center $\mathbf{c}_k = [c_{1,k}, c_{2,k}, \dots, c_{N,k}]$ lies in the N -dimensional space of pre-processed CQI reports. The clustering objective is to minimize the average distortion, defined as the mean squared Euclidean distance between each data point $\mathbf{y}_{u,M}$ and its assigned cluster centroid $\mathbf{c}_{k(u)}$:

$$d(\mathcal{K}) = 1/U_M \sum_{u=1}^{U_M} |\mathbf{y}_{u,M} - \mathbf{c}_{k(u)}|^2, \quad (16)$$

where $\mathbf{c}_{k(u)}$ is the closest center to $\mathbf{y}_{u,M}$. This minimization can be achieved using classical clustering techniques such as K-Means or more robust alternatives like Swap heuristics [17], iteratively refining the center set $\mathcal{K}_M^{(z)}$ over $z = 1, 2, \dots, Z_C$. These methods serve as the foundation for the proposed SAST-based optimization strategy presented in Section II-B.4.

1) *Iterative K-means Algorithm*: At each iteration z , K-means performs:

a) Assignment: each data point $\mathbf{y}_{u,M} \in \mathcal{U}_M$ is assigned to its nearest center $\mathbf{c}_k^{(z-1)} \in \mathcal{K}^{(z-1)}$, forming neighborhoods \mathcal{N}_k ; *b*) Update: new centers are computed as the mean of their assigned points:

$$\bar{\mathbf{c}}_k^{(z-1)} = 1/|\mathcal{N}_k| \cdot \sum_u^{|\mathcal{N}_k|} \mathbf{y}_{u,M}, \quad (17)$$

and set as $\mathbf{c}_k^{(z)} = \bar{\mathbf{c}}_k^{(z)}$;

c) Reassignment: data points are reassigned to the updated nearest centers. This loop continues for Z_C iterations or until convergence. Two main challenges arise: (i) neighborhood search becomes computationally expensive as U_M increases, which can be mitigated using KN-trees for faster lookup [35]; (ii) convergence to local minima, inherent in K-means, can be improved through enhanced initialization of centers and convergence criteria.

2) *KN-Tree Accelerated Clustering*: To address the complexity of K-means clustering for large CQI datasets, we adopt a KN-tree structure to accelerate the neighborhood search. The KN-tree recursively partitions the N -dimensional pre-processed CQI space by orthogonal splits along median coordinates. In Fig. 3, an example with $N = 2$ and $U_M = 21$ data points is shown. Initially, points are sorted along the first dimension ($0X$), and the median point \mathbf{y}_1 becomes the root node. The left and right subsets are then recursively split along alternating coordinates ($0Y$, $0X$, etc.), generating a binary tree of nested axis-aligned bounding boxes.

Each node in the KN-tree corresponds to a sub-region (cell) and contains either a single point (leaf) or an internal node that defines a local split. During each K-means iteration z , a candidate center set $\mathcal{C}_u^{(z)} \subseteq \mathcal{K}_M^{(z)}$ is maintained for every node $\mathbf{y}_{u,M} \in \mathcal{U}_M$ to reduce the search space. The filtering process works as follows:

- (i) The midpoint of the cell is computed, and the closest center \mathbf{c}_* is selected.
- (ii) For any other center $\mathbf{c} \in \mathcal{K}_M^{(z)} \setminus \{\mathbf{c}_*\}$, the vertex v_u of the cell in the direction of $\bar{\mathbf{c}}_* \bar{\mathbf{c}}$ is determined based on the min/max projection along each dimension.

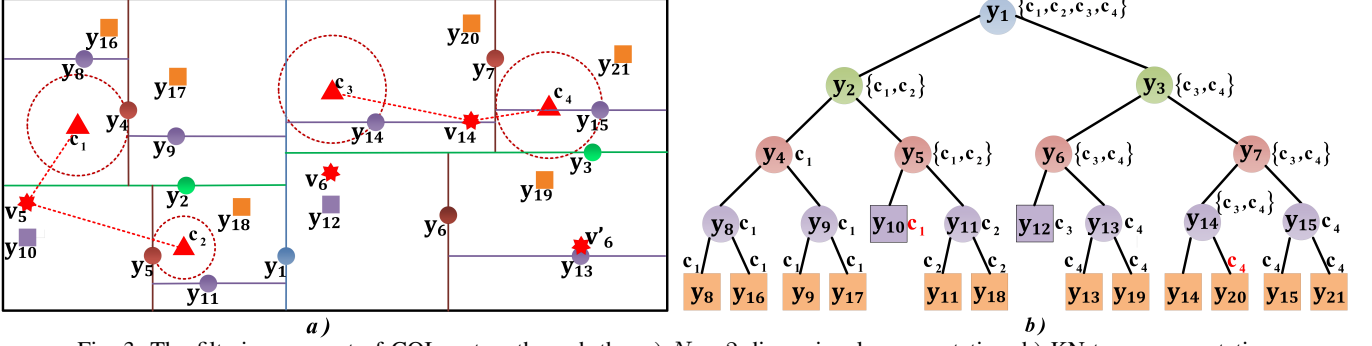


Fig. 3: The filtering concept of CQI centers through the: a) $N = 2$ dimensional representation; b) KN-tree representation.

(iii) The center c is retained in $\mathcal{C}_u^{(z)}$ only if $d(c_*, v_u) < d(c, v_u)$.

If a node retains a single candidate c_* , its centroid is directly assigned to that center. Otherwise, filtering continues through child nodes. Once all data points are associated with centers, the neighborhood $\mathcal{N}_k^{(z)}$ of each center is formed, and the updated centroid is calculated as in 17. Fig. 3.a shows $K = 4$ centers and corresponding candidate filtering in the KN-tree. For example, y_5 is closer to c_2 by midpoint, but its vertex v_5 is closer to c_1 , leading to assignment to c_1 . Similar behavior is seen for y_6 and y_{14} , showing how the filtering ensures better center assignments.

This KN-tree-enhanced clustering strategy significantly improves efficiency by reducing the number of center comparisons per node and accelerates convergence of K-means toward a lower-distortion configuration.

3) *Center Refinement and Swap-Based Initialization*: To enhance convergence toward better clustering solutions, K-means iterations are organized into runs or epochs. Each run begins with an initial center set \mathcal{K}_M^0 . If at iteration z , the distortion $d(\mathcal{K}_M^{(z)})$ improves over $d(\mathcal{K}_M^0)$ and meets a defined threshold, the run is marked successful, and $\mathcal{K}_M^{(z)}$ becomes the new initial set for the next run. Otherwise, if the improvement is insufficient after the maximum allowed iterations, the run is unsuccessful and the centers are randomly re-initialized from \mathcal{U}_M . The best set of centers found so far is tracked as:

$$\mathcal{K}_M^* = \begin{cases} \mathcal{K}_M^{(z)}, & d^{(z)} < d^* \\ \mathcal{K}_M^*, & \text{otherwise,} \end{cases} \quad (18)$$

where d^* is the lowest distortion observed. Despite refinements, this method remains a local search, making it prone to convergence at local minima.

To mitigate this, Swap heuristics are introduced, where each center $c_k \in \mathcal{K}_M^{(z)}$ is randomly selected from the dataset \mathcal{U}_M , i.e., $\mathcal{K}_M^{(z)} \subset \mathcal{U}_M$. This randomization increases exploration potential and reduces the risk of local traps, though it may require more iterations to converge.

4) *Proposed SAST Meta-Heuristic Clustering*: To balance the exploration capabilities of random center selection and the precision of KN-tree-based clustering, we propose a meta-heuristic algorithm that dynamically switches between both strategies. Unlike conventional KN-tree clustering, which discards non-improving center sets, our approach evaluates whether such sets might still guide the search toward better solutions. Similarly, while random center selection can escape local minima, it often yields high distortion. By alternat-

Algorithm I: SAST-based Clustering

```

1: while ( $run_{new} = true$ ) & ( $z \leq Z_C$ ) do
2:   start iteration  $z$ 
3:   if ( $random = true$ )
4:     randomize one center  $\forall c_k \in \mathcal{K}_M^{(z-1)}$ ,  $k = 1, \dots, K_M$ 
5:   else iterated KN-tree
6:     determine neighborhood  $\mathcal{N}_k$  for each  $c_k \in \mathcal{K}_M^{(z-1)}$ 
7:     based on the filtering approach
8:     calculate centroid  $\bar{c}_k^{(z)}$  based on (17) and  $c_k^{(z)} = \bar{c}_k^{(z)}$ 
9:   end if
10:  assign each point  $y_{u,M} \in \mathcal{U}_M$  to closest  $c_k \in \mathcal{K}_M^{(z)}$ 
11:  calculate distortion  $d(\mathcal{K}_M^{(z)})$  based on (16)
12:  if ( $z < max_{iterations/run}$ ) or ( $\bar{d}^{(z)} > \bar{d}_{min}$ )
13:     $run_{new} = false$ 
14:  calculate  $\mathbb{P}(\mathcal{K}_{M,1}^{(z)} | \mathcal{K}_{M,1}^{(z-1)})$  based on (4)-(6)
15:  decrease temperature based on (7)-(8)
16:  if [ $\mathbb{P}(\mathcal{K}_{M,1}^{(z)} | \mathcal{K}_{M,1}^{(z-1)}) > \mathbb{P}_{rand}$ ]:  $random = true$ 
17:    else:  $random = false$ 
18:  else
19:     $run_{new} = true$ ,  $random = true$ 
20:    calculate  $\mathbb{P}(\mathcal{K}_M^{(z)} | \mathcal{K}_M^0)$  based on (4)-(6)
21:    decrease temperature  $T_{old}$  based on (7)-(8)
22:    if ( $d^{(z)} < d^*$ )  $d^* = d^{(z)}$  based on (18)
23:    if ( $\mathbb{P}(\mathcal{K}_M^{(z)} | \mathcal{K}_M^0) > \mathbb{P}_{rand}$ )
24:      Initial set for the next run epoch:  $\mathcal{K}_M^0 = \mathcal{K}_M^{(z)}$ 
25:    else keep  $\mathcal{K}_M^0$  in next run
26:  end if
27: end iteration  $z$ 
28: end while

```

ing between methods and making probabilistic decisions on whether to retain or switch center sets, our framework aims to efficiently discover better clustering configurations.

At each iteration z , given the previous set of centers $\mathcal{K}_M^{(z-1)}$, we solve the following optimization problem to compute the new set $\mathcal{K}_M^{(z)}$, as follows:

$$\min_{\alpha, \beta, \gamma} \sum_{u=1}^{U_M} \sum_{k=1}^{K_M} \alpha_{u,k} \cdot \left\| \mathbf{y}_u - \sum_{l=1}^2 \eta_{k,l} \sum_{r=1}^U \beta_{k,l} \cdot \gamma_{k,r} \cdot \mathbf{y}_r \right\|^2 \quad (19)$$

where:

- $\alpha_{u,k} \in \{0, 1\}$ assigns data point u to center k .
- $\beta_{k,l} \in \{0, 1\}$ selects the clustering method $l \in \{1 \text{ (random)}, 2 \text{ (KN-tree)}\}$ for center j .
- $\gamma_{k,r} \in \{0, 1\}$ indicates whether point r contributes to computing center k .
- $\eta_{k,l} = \begin{cases} 1, & \text{if } l = 1 \\ 1/|\mathcal{N}_k|, & \text{if } l = 2 \end{cases}$ is a normalization factor depending on the clustering method.

This objective balances assignment accuracy based on average distortion, method flexibility, and adaptive center selection,

forming the basis of our SAST-driven clustering procedure.

The proposed SAST-based clustering leverages temperature-driven probabilistic transitions between two strategies: random center selection and KN-tree-based refinement. Let $\mathcal{K}_{M,1}^{(z)}$ denote the set of centers at iteration z obtained using random selection. At each iteration, the state pair $(\mathcal{A}, \mathcal{B}) = (\mathcal{K}_{M,1}^{(z)}, \mathcal{K}_{M,1}^{(z-1)})$ is evaluated. If the distortion $d(\mathcal{K}_{M,1}^{(z)}) \leq d(\mathcal{K}_{M,1}^{(z-1)})$, the random strategy is retained. Otherwise, SAST computes the acceptance probability $\mathbb{P}(\mathcal{A}|\mathcal{B})$, which decreases as temperature cools, favoring a switch to KN-tree-based clustering. In a similar manner, when a run terminates with $d(\mathcal{K}_M^{(z)}) > d(\mathcal{K}_M^0)$, the state pair $(\mathcal{A}, \mathcal{B}) = (\mathcal{K}_M^{(z)}, \mathcal{K}_M^0)$ is evaluated to decide whether to carry over the current centers or reinitialize them.

Algorithm I presents the proposed SAST-based meta-heuristic approach designed to efficiently cluster large datasets \mathcal{U}_M containing pre-processed CQI reports. Each execution begins with a random selection of initial centers, followed by the assignment of data points to their respective clusters. If neither the maximum number of iterations per run has been reached nor the minimum distortion value achieved, the algorithm evaluates whether to switch to the KN-tree-based clustering method, as indicated in lines (13)-(17). If the maximum number of iterations for a run is reached, the current iteration becomes the final one for that run, and the SAST method determines whether to store a new initial set of centers for the subsequent run (lines (19)-(25)). This process continues iteratively until the max number of runs is completed.

Upon completion, the best solution \mathcal{K}_M^* is sorted according to CQI quality. Consider the baseline set \mathcal{U}_1 of top-1 CQI reports with $U_1 = N$, where $\mathbf{y}_{1,1} = [1, 0, \dots, 0]$ and $\mathbf{y}_{N,1} = [0, \dots, 0, 1]$ correspond to the worst and best CQI, respectively. For each center $\mathbf{c}_k \in \mathcal{K}_M^*$, define the nearest CQI index as follows:

$$n_k = \arg \min_{n \in \{1, \dots, N\}} \|\mathbf{c}_k - \mathbf{y}_{n,1}\|^2. \quad (20)$$

Then, define the ordering permutation π such that $n_{\pi(1)} < n_{\pi(2)} < \dots < n_{\pi(K_M)}$. The final ordered center set is:

$$\mathcal{K}_M = \{\mathbf{c}_{\pi(k)}\}_{k=1}^{K_M}, \quad (21)$$

ensuring that $\mathbf{c}_{\pi(1)}$ and $\mathbf{c}_{\pi(K_M)}$ represent the clusters of worst and best average channel conditions, respectively.

C. Supervised Machine Learning

The role of supervised learning is to construct a prediction model that assigns each pre-processed CQI report $\mathbf{y}_{i,M}$, for user $i \in \mathcal{I}_t$, to a corresponding discrete pattern. Define the set of patterns as $\mathcal{P} = \{\mathbf{p}_1, \mathbf{p}_2, \dots, \mathbf{p}_K\}$, where each pattern $\mathbf{p}_k = [p_{k,1}, p_{k,2}, \dots, p_{k,O}]$ is a binary encoding of the cluster index k derived from center $\mathbf{c}_k \in \mathcal{K}_M$, with 0 values replaced by -1 such that $p_{k,o} \in \{-1, 1\}$ for $o = 1, \dots, O$. Given the collection of pre-processed CQI vectors \mathcal{U}_M , the goal is to learn a mapping from the continuous input space to the finite label space \mathcal{P} , using the labeled dataset:

$$\mathcal{V} = \{(\mathbf{y}_u, \mathbf{p}_u) | \mathbf{y}_u \in \mathcal{U}_M, \mathbf{p}_u \in \mathcal{P}, u = 1, \dots, U_M\}. \quad (22)$$

Based on the labeled dataset \mathcal{V} , the goal is to learn a non-linear function $\Phi : \mathbb{R}^N \rightarrow [-1, 1]^O$ that maps each pre-processed CQI vector $\mathbf{y}_{u,M}$ to its corresponding pattern \mathbf{p}_u :

Algorithm II: SAST-based RBFN Training

```

1: for each run epoch (TTI  $t$ )
2:  $\mathcal{V} = false$ 
3:   for each iteration  $z$  (user  $i \in \mathcal{I}_t$ )
4:     receive CQI report  $\mathbf{x}_i$ 
5:     process  $\mathbf{x}_i$  to  $\mathbf{y}_{i,M}$  based on (9)-(15)
6:     if ( $\mathcal{V} = false$ ) pick  $\mathbf{y}_{i,M} \in \mathcal{Y}_M$  from environment
7:     else pick  $\mathbf{y}_{u,M} \in \mathcal{U}_M \forall u = 1, 2, \dots, U_M$ 
8:     determine pattern  $\mathbf{p} \in \mathcal{P}$  for the selected  $\mathbf{y}_M$ 
9:     propagate  $\mathbf{y}_M$  through RBFN based on (23)-(25)
10:    calculate error  $e^{(z-1)}$  based on (27) and (28)
11:    back-propagate error vector  $\mathbf{e}^{(z)}$  based on (30)
12:    correct weights  $\mathcal{W}^{(z-1)}$  based on (31)
13:    calculate error  $e^{(z)}$  based on (29) and (30)
14:    determine prob.  $\mathbb{P}(\mathcal{W}_1^{(z)} | \mathcal{W}_1^{(z-1)})$  based on (4)-(6)
15:    if [ $\mathbb{P}(\mathcal{W}_1^{(z)} | \mathcal{W}_1^{(z-1)}) > \mathbb{P}_{rand}$ ] then  $\mathcal{V} = false$ 
16:    else  $\mathcal{V} = true$ 
17:    if iteration  $z = I_t$ 
18:      if  $e^{(z)} < e^0$ 
19:        verify in (29) if  $\mathcal{W}^* = \mathcal{W}^{(z)}$  and set  $\mathcal{W}^0 = \mathcal{W}^{(z)}$ 
20:        else // non-better  $\mathcal{W}^{(z)}$  acceptance
21:          determine  $\mathbb{P}(\mathcal{W}^{(z)} | \mathcal{W}^0)$  based on (4)-(6)
22:          if [ $\mathbb{P}(\mathcal{W}^{(z)} | \mathcal{W}^0) > \mathbb{P}_{rand}$ ] then  $\mathcal{W}^0 = \mathcal{W}^{(z)}$ 
23:          else keep previous  $\mathcal{W}^0$ 
24:        end if
25:        reduce temperature  $\mathbf{T}_{old}$  based on (7)-(8)
26:      end if
27:    end iteration  $z$ 
28: end run epoch

```

$$\Phi(\mathbf{y}_{u,M}) = \mathbf{p}_u, \quad u = 1, \dots, U_M. \quad (23)$$

This mapping is implemented using a RBF network:

$$\Phi(\mathbf{y}_{u,M}) = \Phi_2 [\mathbf{W} \cdot \Phi_1(\mathbf{y}_{u,M}^T)], \quad (24)$$

where $\mathbf{W} = \{w_{k,o}\}$ is the matrix connecting the K hidden units to O output nodes. The hidden layer output is the vector $\Phi_1 = [\phi_{u,1}^{(1)}, \dots, \phi_{u,K}^{(1)}]$, where each ϕ is a Gaussian RBF:

$$\phi_{u,k}^{(1)} = \exp\left(-\frac{\|\mathbf{y}_{u,M} - \mathbf{c}_k\|^2}{2\sigma^2}\right), \quad (25)$$

with fixed $\sigma > 0$. Finally, $\Phi_2 = [\phi_1^{(2)}, \dots, \phi_O^{(2)}]$ applies a $\tanh(\cdot)$ activation function component-wise at the output layer.

Perfect interpolation in (23) is generally unattainable due to the impracticality of collecting the complete space of CQI vectors \mathcal{U}_M , as many combinations are never observed under realistic channel fading conditions. Therefore, the RBF-based mapping Φ is approximated as $\tilde{\Phi}$. To improve generalization, we construct a new training set \mathcal{T} using CQI reports $\mathbf{y}_{i,M} \in \mathcal{Y}_M$ gathered from network simulations:

$$\mathcal{T} = \{(\mathbf{y}_{i,M}, \mathbf{p}_i) | \mathbf{y}_{i,M} \in \mathcal{Y}_M, \mathbf{p}_i \in \mathcal{P}\}. \quad (26)$$

For samples in $\mathcal{T} \setminus \mathcal{V}$, the model employs:

$$\tilde{\Phi}(\mathbf{y}_{i,M}) + E(\mathcal{W}, \mathbf{y}_{i,M}) = \mathbf{p}_i, \quad (27)$$

where E denotes the approximation error as a function of weights from set \mathcal{W} . Integrating this training with a network simulator allows the RBF model to adaptively learn under realistic CQI variations and better generalize beyond the original labeled set \mathcal{V} .

Similarly, the RBF network is trained over Z_R iterations grouped into epochs aligned with TTIs. At each iteration $z \in \{1, 2, \dots, Z_R\}$, the goal is to minimize the mean square error:

$$e^{(z)} = 1/O \cdot \|\mathbf{p}_i - \mathbf{y}_{i,M}^{(2)}\|^2 = 1/O \cdot \sum_o (p_{i,o} - y_{i,o}^{(2)})^2, \quad (28)$$

where $\mathbf{y}_{i,M}^{(2)} = \Phi_2(\cdot)$ is the RBF output vector. The best set of weights \mathcal{W}^* is updated according to:

$$\mathcal{W}^* = \begin{cases} \mathcal{W}^{(z)}, & \text{if } e^{(z)} < e^* \\ \mathcal{W}^*, & \text{otherwise,} \end{cases} \quad (29)$$

where e^* is the lowest error observed so far. Each iteration includes: *a)* forward pass of \mathbf{y}_M , *b)* error computation and backpropagation, and *c)* weight update to avoid local minima.

1) *Forward Propagation.*: The output $\mathbf{y}_M^{(2)}$ is computed from input \mathbf{y}_M and weights $\mathcal{W}^{(z)}$. To avoid overfitting from relying solely on \mathcal{T} , we alternate between \mathcal{T} and \mathcal{V} using a SAST-driven management controller. Each run starts with \mathcal{T} and switches to \mathcal{V} based on energy states $\mathcal{A} = \mathcal{W}_1^{(z)}$ and $\mathcal{B} = \mathcal{W}_1^{(z-1)}$, with $f = e$, $f^* = e^*$. If $F(\mathcal{W}_1^{(z)}) \geq F(\mathcal{W}_1^{(z-1)})$, training continues with \mathcal{T} ; otherwise, $\mathcal{W}_1^{(z)}$ is accepted with probability $\mathbb{P}(\mathcal{W}_1^{(z)}|\mathcal{W}_1^{(z-1)})$. If this is less than \mathbb{P}_{rand} , the switch to \mathcal{V} occurs from iteration $z + 1$.

2) *Error Back-Propagation.*: For each training sample from \mathcal{T} or \mathcal{V} , the input \mathbf{y}_M produces the output $\mathbf{y}_M^{(2)}$ via forward propagation. The error vector $\mathbf{e} = \mathbf{p} - \mathbf{y}_M^{(2)}$ is computed and back-propagated through the output layer using:

$$\mathbf{e}^{(2)} = \nabla\Phi^{(2)} \circ \mathbf{e}, \quad (30)$$

where $\nabla\Phi^{(2)}$ is the vector of derivatives of the activation functions, and \circ denotes element-wise multiplication. Let $\mathbf{y}_M^{(1)}$ be the hidden layer output and $\mathbf{W}^{(z-1)}$ the previous weight matrix, the weights are updated by:

$$\mathbf{W}^{(z)} = \mathbf{W}^{(z-1)} + \eta \cdot \mathbf{y}_M^{(1)T} \times \mathbf{e}^{(2)}, \quad (31)$$

where η is the learning rate.

3) *Acceptance of RBFN Weights.*: To avoid convergence to local minima, each run epoch (TTI) begins with an initial weight set \mathcal{W}^0 , which may be updated over I_t iterations to yield $\mathcal{W}^{(z)}$. The SAST-based management controller evaluates $\mathcal{A} = \mathcal{W}^{(z)}$, $\mathcal{B} = \mathcal{W}^0$, with $f = e$ and $f^* = e^*$. If $F(\mathcal{W}^{(z)}) \leq F(\mathcal{W}^0)$, then $\mathcal{W}^{(z)}$ is accepted as the initial set for the next run. Otherwise, if $F(\mathcal{W}^{(z)}) > F(\mathcal{W}^0)$, the non-better solution is accepted with probability $\mathbb{P}(\mathcal{W}^{(z)}|\mathcal{W}^0)$; it is retained only if this exceeds a random threshold \mathbb{P}_{rand} . If not, \mathcal{W}^0 is restored. The initial temperature \mathbf{T}_0 is computed over L iterations as in (7), and gradually decreased using (8) at each TTI. Algorithm II details the full RBFN-based CQI classification training process.

D. Statistical Stage

At each TTI t , the classifier outputs the vector from (15), where $v_{M,k} \in [0, 1]$ denotes the normalized number of users in class k , with $\sum_k^K v_{M,k} \leq 1$ due to possible CQI delays or losses. Once parameters $\{M, K, \sigma, \eta\}$ are set and the RBF network is trained, classification can be offloaded to the mobile equipment. Reporting only the class index k significantly reduces signaling overhead, while still enabling accurate CQI reconstruction at the base station when K is sufficiently large. Additionally, dual reporting (class index and CQI vector) allows error correction by cross-referencing the two representations.

As shown in Fig. 2, the classification vector \mathbf{v}_M is integrated into the controller state $\mathbf{s} \in \mathcal{S}$, alongside $\{\alpha_{t-1}, \beta_{t-1}, \mathbf{\Gamma}, I_t\}$, to estimate the fairness parameters $[\alpha_t, \beta_t]$ at each TTI t and ensure management feasibility. When the number of CQI

classes K increases, \mathbf{v}_M may dominate the state, making feature extraction essential. The controller's decisions are guided by the sensitivity of α_t and β_t to changes in \mathbf{v}_M under NGMN fairness constraints. For instance, poor CQI distributions lead to $\alpha_t > \beta_t$ to favor fairness, whereas favorable distributions yield $\alpha_t < \beta_t$ to enhance throughput. Additionally, low dispersion in \mathbf{v}_M permits reducing α_t to optimize capacity, while high dispersion requires increasing it to maintain fairness compliance.

To reduce the dimensionality of the classification vector \mathbf{v}_M and retain its key characteristics, we extract a set of descriptive features. Let $h_k[t] \in \{0, 1\}$ indicate if class k is active at TTI t , such that $h_k[t] = 1$ if $v_{M,k} > 0$, and $h_k[t] = 0$ otherwise. The total number of active classes is:

$$h_a = \sum_{k=1}^K h_k. \quad (32.a)$$

The class dispersion is measured by:

$$\sigma_a = 1/h_a \cdot \sum_{k=1}^K h_k \cdot (v_{M,k} - 1/h_a)^2. \quad (32.b)$$

To quantify the CQI quality over all vehicular users every TTI, we define a support set $\mathcal{Q} = \{\bar{\mathbf{v}}_k\}$, where each $\bar{\mathbf{v}}_k$ is a one-hot vector. The best match to the current \mathbf{v}_M is found by minimizing the Euclidean distance:

$$d(\mathbf{v}_M, \bar{\mathbf{v}}_k) = d_{M,k} = \|\mathbf{v}_M - \bar{\mathbf{v}}_k\|, k = 1, 2, \dots, K, \quad (32.c)$$

and then, let $k_{\bar{\mathbf{v}}}$ be the index of the nearest support vector

$$k_{\bar{\mathbf{v}}} = \operatorname{argmin}_{k'} d(\mathbf{v}_M, \bar{\mathbf{v}}_{k'}). \quad (32.d)$$

and $d_{M,k}$ the associated distance. Based on the proposed compression mechanism, instead of the full vector \mathbf{v}_M , the controller uses the compact feature vector $[h_a, \sigma_a, d_{M,k}, k_{\bar{\mathbf{v}}}]$. The state vector becomes from (3) becomes:

$$\mathbf{s} = [\alpha_{t-1}, \beta_{t-1}, \mathbf{\Gamma}, h_a, \sigma_a, d_{M,k}, k_{\bar{\mathbf{v}}}, I_t] \in \mathcal{S}. \quad (33)$$

IV. SIMULATION RESULTS

The enhanced network simulator [11], [36] supports the proposed CQI compression framework under two main settings: *Online* (real-time processing) and *Offline* (algorithm optimization). These settings are divided into four functional modes:

- *CQI Collection & Pre-processing (Online)*: Gathers and processes CQI data for unique, representative samples (Section III-A).
- *Clustering Analysis (Offline)*: Applies the SAST-based metaheuristic for offline clustering and benchmarking (Section III-B).
- *RBFN Training (Online)*: Trains and updates the RBF network using dynamic CQI data (Section III-C).
- *Management & Evaluation (Online)*: Employs compressed representations to support RL-based management controller meeting fairness and throughput goals (Sections II-A, III-D).

A. Data Collection

We simulate a 20 MHz cellular system ($J = 100$) with 19 cells and 1000 users moving at 120 km/h under Jakes fading, as detailed in Table I. CQI reports are periodically and reliably received. To reduce redundancy and complexity, we apply a

TABLE I: Parameter Settings

Parameter	Value/Description
Network Parameters	
Downlink Transmission Power	43dBm
Multipath Fading Model	Jakes Model with 12 Paths
Path Loss Model	Macro Cell Urban Area
Penetration Loss	10 dB
Shadowing Loss Mean/Deviation	$\mu = 0, \sigma = 8dB$
Noise Figure (F)	2.5
Noise Spectral Density	-174dBm
Number of Cells / Reuse Factor	19/3
RB Bandwidth	180KHz
CQI Reporting Mode	Periodic, every 1ms
PUCCH Channel	Errorless
Number of CQI Feedbacks per TTI	1000
User Speed	120 km/h
User Mobility Model	Random Direction
Bandwidth	20MHz
Target BLER	10%
CQI Preprocessing Mode	$M \in \{3, 4, 5\}$
Collection Size(U_M)	$U_3 = 33596, U_4 = 144179,$ $U_5 = 206473$
SAST-based Clustering Parameters	
Max Iterations per Run	10
Total Number of Iterations (Z_C)	1000
Minimum Distortion (\bar{d}_{min})	0.1
Acceptance Probability (\mathcal{K}) (\mathbb{P}_0)	0.5
Acceptance Probability (K-Means)	0.5
Temperature Running Length (L)	10
Temp. Reduction Factor (R_T)	0.95
Tunneling Parameter (ω)	0.02
Number of Centers (K)	$K \in \{64, 128, 256, 512\}$
SAST-based RBFN Training Parameters	
Max Iterations per Run	1000
Total Number of Iterations (Z_C)	10^6
Acceptance Probability (\mathcal{V}) (\mathbb{P}_0)	0.8
Acceptance Probability (Weights)	0.8
Temperature Running Length(L)	50000
Temp. Reduction Factor(R_T)	0.99
Tunneling Parameter(ω)	0.1
RBFNN Output Layer Function	Tangent Hyperbolic
Gaussian Parameter (σ)	see TABLE III
Learning Rate (η)	see TABLE III
Intelligent Management Controller Parameters	
Frame Structure	FDD
CQI Reporting Mode	Full-band, periodic per TTI
PUCCH Model	Errorless
Scheduler Type	GPF-SP / GPF-DP
Traffic Type	Best Effort
RLC ARQ	No Retransmissions
NGMN Confidence Factor	0.05
Controller Timescale	1 TTI
Number of Users (I_t)	Variable: 15-120
RL Algorithms	Q-L, DoubleQ-L, SARSA, QV, QV2, QVMAX, QVMAX2, ACLA, CACLA1, CACLA2
Training/Testing Time	3000s/200s (in average)
Neural Network Type	Feed-Forward
No. of hidden layers / nodes	1/60

pre-processing step selecting the top M CQI features ($M = \{3, 4, 5\}$), followed by a uniqueness check. Smaller M values yield compact state spaces, eliminating the need for clustering or classification. Data collection runs in parallel for each M , with a stopping criterion defined using:

$$u_{M,t} = (1 - \beta)u_{M,t-1} + \beta \cdot \left[I_t - \frac{U_{M,t} - U_{M,t-1}}{I_t} \right], \quad (34)$$

where $\beta = 0.005$. Collection stops when $u_{M,t} > 0.99$, signaling saturation. The resulting dataset sizes are: $U_3 = 33596$,

$U_4 = 144179$, and $U_5 = 206473$, used in offline clustering and online RBFN training.

B. Performance Analysis of Proposed SAST-based Clustering

Based on the datasets \mathcal{U}_3 , \mathcal{U}_4 , and \mathcal{U}_5 , the proposed SAST-based clustering method is applied to compute the corresponding data center sets \mathcal{K}_3 , \mathcal{K}_4 , and \mathcal{K}_5 . Its performance is compared against several clustering baselines: KN-tree-based k-means (KN), random center selection (RS), a hybrid RS-KN approach (RSKN), and simulated annealing (SA). KN uses neighborhood-based centroid updates; RS selects centers randomly at each iteration; RSKN performs a single RS step per run before switching to KN updates; and SA minimizes the distortion function $F(\mathcal{X})$ via probabilistic transitions, similar to SAST but without stochastic tunneling.

In offline mode, each clustering algorithm runs for a maximum of $Z_C = 1000$ iterations, organized into 100 runs of 10 iterations each. For SAST and SA, the initial acceptance probability is $\mathbb{P}_0 = 0.5$, governing both RS-to-KN transitions and acceptance of non-improving solutions. A cooling rate of $R_T = 0.95$ gradually reduces randomness, favoring KN-based refinement in later stages. SAST introduces an early termination condition: if the distortion improvement within a run falls below a threshold ($d^{(z)} - d^0 < \bar{d}_{min} = 0.1$), the run ends early, enabling more frequent resets and efficient exploration. The tunneling factor $\omega = 0.02$ balances exploration and exploitation: larger values mimic RS behavior by over-accepting non-improving centers, while smaller values risk early convergence to KN-like local minima. This setting ensures convergence toward global optima within 50 iterations. All parameter values are listed in Table I.

The clustering performance is evaluated for center sizes $K = \{64, 128, 256, 512\}$ across datasets \mathcal{U}_3 , \mathcal{U}_4 , and \mathcal{U}_5 , assessing how different (M, K) configurations affect algorithm behavior. The analysis focuses on distortion and CPU time to compare the efficiency and accuracy of each method, particularly under varying SAST parameter settings. Table II summarizes these results: KN serves as the baseline with absolute values, while other methods are compared by their percentage change in distortion and runtime. This allows for an informed assessment of how clustering quality scales with system complexity and impacts downstream resource management.

Across all configurations, the KN-tree implementation proves computationally efficient, offering CPU times similar to the RS method, despite its centroid refinement step. As expected, increasing M or K raises the complexity across all algorithms. Still, the proposed SAST method strikes the best balance between computational cost and clustering distortion. In terms of distortion, RS consistently performs worse due to its random center selection strategy, which lacks refinement. Hybrid methods improve upon KN, confirming its tendency to converge to local minima. RSKN, while simpler, offers moderate gains but lacks flexibility due to its fixed switching logic. In contrast, the SAST algorithm, with its dynamic tunneling mechanism, achieves the lowest distortion across all configurations. Notably, SAST's advantage grows with higher K for a fixed M , but diminishes as M increases. This trend

TABLE II: Performance Comparison of Clustering Techniques (Average Distortion / CPU Time)

Method	M = 3		M = 4		M = 5	
	K = 64	K = 128	K = 64	K = 128	K = 64	K = 128
KN	0.0193 / 16.09	0.0094 / 25.96	0.0111 / 56.9	0.0065 / 90.25	0.0084 / 137.19	0.0058 / 208.18
RS	28.1% / -1.2%	30.4% / 0.4%	31.2% / 4.5%	32.8% / 2.7%	26.4% / -1.1%	25.2% / 0.9%
RSKN	-1.7% / -1.6%	1.6% / -1.4%	3.4% / -3.8%	2.5% / -3.4%	0.9% / -3.1%	0.2% / -2.3%
SA	-7.1% / -3.3%	-8.1% / -0.9%	-2.4% / -4.1%	-0.8% / -3.6%	-1.5% / -5.7%	-2.5% / -3.5%
SAST	-7.3% / -3.4%	-8.2% / -0.6%	-2.6% / -6.8%	-1.7% / -1.4%	-1.7% / -6.8%	-3.3% / -4.9%

Method	M = 3		M = 4		M = 5	
	K = 256	K = 512	K = 256	K = 512	K = 256	K = 512
KN	0.0045 / 43.44	0.0022 / 75.01	0.004 / 143.03	0.0027 / 223.8	0.0041 / 320.52	0.0029 / 504.21
RS	34.3% / 1.8%	54.3% / 2.5%	29.4% / 1.4%	32.5% / 0.3%	24.4% / -0.9%	27.5% / -2.7%
RSKN	3.2% / -0.4%	-0.5% / 0.8%	-0.8% / -3.5%	-1.2% / -1.3%	0.1% / -1.1%	-0.8% / -1.8%
SA	-7.4% / -0.4%	-5.7% / 1.5%	-4.1% / -2.9%	-3.5% / -1.9%	-3.0% / -2.3%	-2.8% / -1.6%
SAST	-9.4% / -0.2%	-5.9% / 0.7%	-4.3% / -2.2%	-3.9% / -1.9%	-3.2% / -2.3%	-3.3% / -1.9%

TABLE III: Learning Rate and Gaussian Parameter for Different K and M Values

K	M=3		M=4		M=5	
	η	σ	η	σ	η	σ
64	0.089	50	0.05	90	0.032	120
128	0.075	130	0.063	180	0.01	180
256	0.072	270	0.021	210	0.007	230
512	0.022	440	0.006	370	0.002	310

indicates that low-dimensional pre-processing (e.g., $M = 3$) is sufficient for effective clustering and subsequent resource management, making it a preferred choice for efficient CQI compression.

C. Performance of Proposed SAST-based RBFN Training

The sets of centers \mathcal{K}_3 , \mathcal{K}_4 , and \mathcal{K}_5 , computed via SAST for $K = \{64, 128, 256, 512\}$, are used as activation centers in separate RBF networks. Each RBFN is trained online for its corresponding configuration, enabling dynamic integration of historical CQI data ($\mathcal{U}_3, \mathcal{U}_4, \mathcal{U}_5$) with newly generated reports from the network simulator. This training strategy improves the model's generalization and supports robust classification of pre-processed CQI reports into quality patterns across diverse operational conditions.

To train the RBF networks, we simulate a vehicular network with $I_t = 1000$ users reporting CQI values at each TTI while moving at 120 km/h, using the configuration parameters from Table I. The 1000 CQI reports received per TTI are pre-processed for $M = \{3, 4, 5\}$ to form the training set \mathcal{T} as in Eq. (26). To avoid overfitting, particularly when users experience prolonged similar channel conditions, the SAST metaheuristic is applied during training to escape local minima and improve weight updates. A total of $Z_R = 10^6$ iterations are performed, structured into 1000 runs (epochs) with 1000 iterations each (aligned with the number of CQI samples per TTI). Within each run, SAST adaptively switches between \mathcal{T} and \mathcal{V} and decides whether to retain the current weight configuration for initialization in the next run, effectively balancing exploration and exploitation during training.

To facilitate stable RBFN training, the initial acceptance probability for both data switching and weight updates is set

to $\mathbb{P}_0 = 0.99$, with a temperature decay rate of $R_T = 0.99$, enabling gradual cooling across the high iteration count. A tunneling factor $\omega = 0.1$ ensures broad exploration over 10 training runs (10,000 samples). Early training emphasizes exploration by favoring the dataset \mathcal{T} and accepting sub-optimal weights, promoting diversity in the weight space. As training advances, SAST shifts focus to validation data \mathcal{V} and tightens weight acceptance, allowing only improved solutions to persist. This adaptive behavior guides the network toward convergence, with full training parameters listed in Table I.

Before training the RBF networks, optimal values for the Gaussian parameter (σ) and learning rate (η) must be determined for each (M, K) configuration. Figure 4 compares error distributions for the proposed SAST-based training (dashed lines) and conventional training on \mathcal{V} alone (solid lines). As expected, SAST yields slightly higher mean errors due to its controlled exploration, which prevents premature convergence and enhances generalization by dynamically integrating both \mathcal{T} and \mathcal{V} samples. Figures 4.a–c show error trends for varying σ (with fixed $\eta = 0.1$) across $M = \{3, 4, 5\}$. Two key observations emerge: (i) increasing the number of centers K reduces error due to improved model expressiveness; (ii) higher M values also reduce error, reflecting the benefits of richer input representations. Notably, optimal σ values shift upward as M and K increase, indicating a need for broader basis functions to ensure smooth generalization in more complex models. Figures 4.d–f analyze error for varying η (with fixed $\sigma = 10$). Here, increasing K leads to higher errors, likely due to over-complexity and limited training data per center. Likewise, increasing M introduces greater input granularity but also raises sensitivity to preprocessing accuracy, slightly elevating error. To identify the best (σ, η) pair for each (M, K) , extensive validation is performed, and the optimal configurations are listed in Table III. These settings are used in the next subsection to compress the CQI states in RL-based management controller.

D. Performance Analysis of RL-Assisted Management Policies

This study analyzes the performance of RL-assisted management policies operating under NGMN fairness constraints, using compressed CQI inputs generated by RBF networks. Different (M, K) configurations are tested to evaluate how

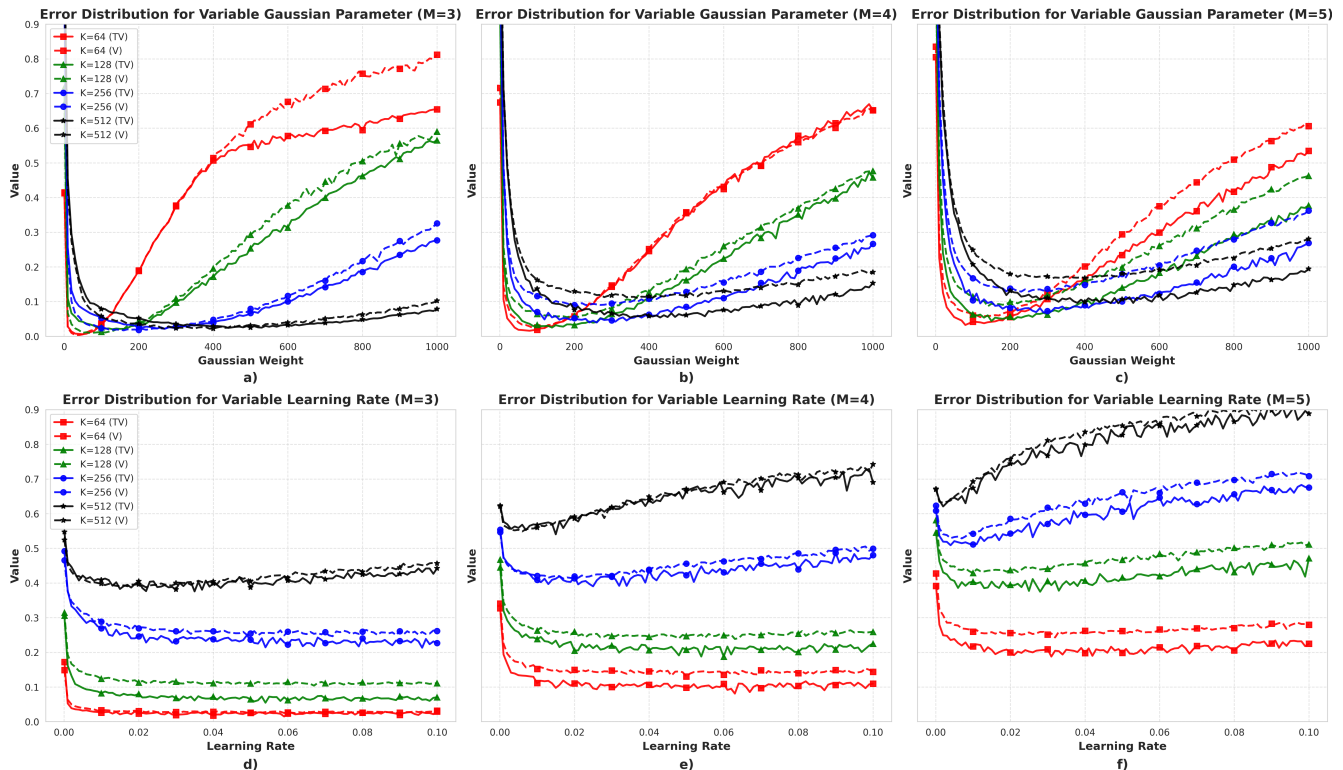


Fig. 4: The Error Distribution for the Gaussian Parameter (σ) when processing top a) $M = 3$, b) $M = 4$, c) $M = 5$ CQI features. The Error Distribution for the Learning Rate (η) when processing top d) $M = 3$, e) $M = 4$, f) $M = 5$ CQI features.

CQI compression affects the RL agents' ability to guide the management controller toward the feasible region \mathcal{FA} , while minimizing time spent in unfair \mathcal{UF} and overfair \mathcal{OF} regions. The goal is to assess the long-term effectiveness of compressed-state RL policies versus their uncompressed counterparts and state-of-the-art approaches in terms of fairness performance.

The simulation scenario features a fast-varying mobile environment with users traveling at 120 km/h. User activity dynamically ranges between 15 and 120 devices, randomly switching between online and idle states. The system employs an FDD structure with periodic full-band CQI reporting and a downlink-only, best-effort traffic model to isolate fairness behavior from traffic-dependent variations. The management policy is based on the Generalized Proportional Fair (GPF) rule, with fairness control handled via either simple parameterization (SP), adjusting a single fairness parameter α_t , or double parameterization (DP), where both α_t and β_t are jointly optimized. To train and evaluate the proposed system, a diverse set of RL algorithms is applied, including Q-Learning, SARSA, Double-Q, QV variants, ACLA, and CACLA [11]. CACLA2 supports continuous DP-based control, while all other RL approaches are used for continuous SP adaptation. These models are trained for 3000 seconds with various (M, K) compression settings and are evaluated over ten 200-second test runs under consistent conditions. The results, averaged across trials, provide a robust comparison of how CQI compression affects the fairness-oriented performance of RL-based management policies.

Table IV presents the evaluation of RL-based management algorithms under multiple configurations defined by the RBFN

parameters (M, K) . Across all settings, CACLA2 achieves higher fairness performance, maintaining over 96% of percentages of TTIs within the feasible region (p_{fa}) and exhibiting minimal time percentage in unfair (p_{uf}) and overfair (p_{of}) states. Notably, CACLA2 reaches its best performance with $(M = 4, K = 512)$, yielding $p_{fa} = 97.76\%$, while maintaining $p_{uf} = 1.88\%$ and $p_{of} = 0.37\%$. In contrast, algorithms like Q-Learning and Double-Q often demonstrate instability, with a tendency to shift the system toward either excessive unfairness or overfairness under certain (M, K) configurations. While methods such as CACLA1, ACLA, and QVMax2 also achieve high fairness, they occasionally trail behind CACLA2 in consistency across configurations. CACLA2 stands out as the most robust algorithm, especially at higher K values, making it suitable for real-time, fairness-aware service-level management; increasing M beyond 4 offers marginal gains, suggesting that selecting the top- $M = 4$ CQI indicators provides sufficient fidelity for state representation in this context.

Figure 5 presents a performance and complexity comparison between CACLA2 ($M = 4, K = \{64, 128, 256, 512\}$) and state-of-the-art resource management strategies including Proportional Fair (PF), Maximizing Throughput (MT), and Adaptive Scheduling (AS) [11]. The PF method, with fixed parameters ($\alpha = 1, \beta = 1$), exhibits extreme overfairness ($p_{of} > 98\%$), while MT and AS achieve feasible region operation in approximately 85% of TTIs and show around 10% in the unfair region. MT adjusts the fairness parameter α_t at each TTI based on the deviation between predicted Jain's Fairness Index (JFI) and a target constraint, whereas AS performs fairness adaptation over periodic TTI windows

TABLE IV: Performance Comparison of RL-based management policies (Mean Percentage of TTIs when the CDF is Located in the Unfair ($\mathcal{U}\mathcal{F}$) / feasible ($\mathcal{F}\mathcal{A}$) / overfair ($\mathcal{O}\mathcal{F}$) Areas

Method	M = 3		M = 4		M = 5	
	K = 64	K = 128	K = 64	K = 128	K = 64	K = 128
Q	11.03 / 86.66 / 2.31	5.53 / 89.59 / 4.88	2.84 / 76.44 / 20.73	8.2 / 65.69 / 26.11	6.25 / 79.86 / 13.89	11.36 / 85.8 / 2.84
D-Q	12.04 / 56.96 / 31.01	3.74 / 80.84 / 15.42	9.51 / 54.82 / 35.67	5.69 / 67.83 / 26.48	9.82 / 86.94 / 3.24	7.34 / 88.74 / 3.93
SARSA	1.94 / 87.96 / 10.11	2.66 / 87.16 / 10.18	2.47 / 90.84 / 6.69	2.02 / 90.74 / 7.24	2.54 / 92.78 / 4.69	5.85 / 90.48 / 3.67
QV	3.43 / 90.53 / 6.04	1.78 / 94.57 / 3.66	5.96 / 91.98 / 2.06	6.62 / 88.74 / 4.65	6.07 / 92.49 / 1.45	1.95 / 93.25 / 4.8
QV2	8.71 / 90.24 / 1.06	3.49 / 87.24 / 9.27	7.95 / 87.54 / 4.51	4.02 / 91.01 / 4.97	3.16 / 93.72 / 3.12	5.53 / 88.16 / 6.31
QVMax	9.91 / 88.04 / 2.06	9.83 / 87.66 / 2.51	10.99 / 87.22 / 1.79	2.61 / 86.87 / 10.52	4.41 / 90.99 / 4.61	3.65 / 88.17 / 8.18
QVMax2	3.64 / 93.79 / 2.56	7.44 / 91.68 / 0.89	8.37 / 89.44 / 2.19	4.38 / 93.12 / 2.49	1.79 / 94.22 / 1.43	3.62 / 92.99 / 3.38
ACLA	4.61 / 90.88 / 4.51	3.36 / 92.69 / 3.95	3.33 / 94.46 / 2.22	4.76 / 92.74 / 2.5	4.98 / 93.58 / 4.59	3.36 / 93.32 / 3.32
CACLA1	2.74 / 96.64 / 0.62	3.94 / 94.87 / 1.19	1.77 / 96.57 / 1.66	1.73 / 94.54 / 3.73	1.77 / 93.65 / 3.99	1.88 / 94.13 / 3.99
CACLA2	2.11 / 96.78 / 1.11	2.12 / 96.16 / 1.73	1.69 / 95.23 / 3.08	2.84 / 96.52 / 0.64	1.69 / 94.64 / 3.67	1.74 / 96.45 / 1.81

Method	M = 3		M = 4		M = 5	
	K = 256	K = 512	K = 256	K = 512	K = 256	K = 512
Q	5.91 / 69.48 / 24.61	25.75 / 72.22 / 2.03	1.64 / 40.02 / 58.34	12.69 / 77.9 / 9.41	10.42 / 84.4 / 5.17	2.79 / 86.25 / 10.96
D-Q	10.87 / 86.78 / 2.36	2.84 / 44.2 / 52.96	6.78 / 88.93 / 4.29	7.44 / 74.67 / 17.89	1.67 / 44.97 / 53.36	4.23 / 90.15 / 5.62
SARSA	1.7 / 84.77 / 13.53	35.25 / 58.13 / 6.63	1.72 / 87.37 / 10.91	1.68 / 83.74 / 14.58	2.74 / 87.69 / 9.56	8.07 / 89.83 / 2.09
QV	4.01 / 94.02 / 1.97	8.49 / 91.13 / 0.39	2.19 / 92.51 / 5.3	5.25 / 89.72 / 5.02	5.81 / 92.05 / 2.14	1.72 / 95.65 / 2.64
QV2	8.93 / 88.59 / 2.48	3.29 / 91.39 / 5.31	11.04 / 85.07 / 3.89	3.12 / 93.21 / 3.67	5.04 / 93.03 / 1.93	2.11 / 95.09 / 2.8
QVMax	1.7 / 64.59 / 33.71	2.49 / 86.17 / 11.34	2.16 / 90.42 / 7.41	5.8 / 89.97 / 4.23	6.58 / 89.56 / 3.86	2.0 / 88.49 / 9.51
QVMax2	2.77 / 93.39 / 3.85	2.46 / 93.42 / 4.12	2.71 / 92.26 / 5.03	2.08 / 95.51 / 2.41	6.33 / 88.3 / 5.37	3.98 / 94.55 / 1.47
ACLA	4.82 / 93.13 / 2.06	4.08 / 94.19 / 1.73	3.89 / 92.89 / 3.22	4.18 / 92.06 / 3.76	3.09 / 93.79 / 3.12	7.3 / 91.48 / 1.22
CACLA1	1.87 / 96.54 / 1.59	5.43 / 93.92 / 0.65	1.88 / 97.34 / 0.79	1.8 / 93.43 / 4.77	1.94 / 96.55 / 1.51	1.89 / 95.66 / 2.45
CACLA2	2.06 / 94.89 / 3.04	1.83 / 96.48 / 1.69	1.89 / 97.54 / 0.58	1.88 / 97.76 / 0.37	1.98 / 96.3 / 1.72	1.75 / 97.42 / 0.83

using user throughput CDFs to reduce computational load. CACLA2 without CQI compression underperforms, yielding unfair outcomes in nearly 18% of TTIs, worse than both MT and AS, highlighting the importance of state space expressiveness. However, incorporating CQI compression through the SCAR framework (RBF-based classification with (M, K) granularity) improves fairness by over 14%, shifting more operation into the feasible region. From a complexity standpoint, PF is the simplest, followed by AS, while MT remains computationally heavy due to continuous per-TTI throughput estimation and fairness recalculation. CACLA2 without compression maintains low complexity close to AS, and although increasing the number of RBF centers (K) steadily adds computational cost, the number of top CQIs considered (M) has negligible impact. Overall, SCAR provides an efficient balance, enabling RL-based management controllers like CACLA2 to outperform traditional schemes in fairness while preserving practical runtime constraints.

V. CONCLUSION

This paper introduced SCAR (State-Space Compression for AI-Based Network Management), a framework designed to improve the scalability and effectiveness of AI-assisted network and service management in dynamic vehicular environments through efficient network state abstraction. Rather than relying on raw, high-dimensional CQI inputs, SCAR employs a hybrid compression strategy that combines K-means clustering with radial basis function networks (RBFNs) to extract compact and informative CQI-derived state representations. This approach significantly reduces computational complexity while preserving the state features most relevant to management decisions. To enhance the robustness and adaptability of the compression pipeline, SCAR integrates simulated annealing with stochastic tunneling (SAST) to optimize both

the clustering process and the RBFN training stage, achieving approximately 10% lower representation distortion compared to baseline methods. When applied to RL-based management policies, the proposed compressed state representations yield substantial performance improvements, including more than a 15% increase in the proportion of decision intervals operating within feasible management regions, highlighting gains in both service-level fairness and overall network efficiency.

By decoupling learning-based management from raw CQI dimensionality and radio-specific assumptions, SCAR provides a technology-agnostic and scalable solution suitable for supporting data-intensive vehicular services such as cloud gaming, augmented reality, and high-definition video streaming. The results demonstrate that compression-aware intelligence at the network edge is a key enabler for effective AI-based network and service management in fast-varying, high-demand vehicular systems.

ACKNOWLEDGMENT

This research was conducted as part of the UKIERI-SPARC project “DigIT—Digital Twins for Integrated Transportation Platform”, grant number UKIERI-SPARC/01/23.

REFERENCES

- [1] G. P. Sharma, D. Patel, J. Sachs, M. De Andrade, J. Farkas, J. Harmatos, B. Varga, H.-P. Bernhard, R. Muzaffar, M. Ahmed, F. Dürr, D. Bruckner, E. M. De Oca, D. Houatra, H. Zhang, and J. Gross, “Toward Deterministic Communications in 6G Networks: State of the Art, Open Challenges and the Way Forward,” *IEEE Access*, vol. 11, pp. 106 898–106 923, 2023.
- [2] G. J. Sutton, J. Zeng, R. P. Liu, W. Ni, D. N. Nguyen, B. A. Jayawickrama, X. Huang, M. Abolhasan, Z. Zhang, E. Dutkiewicz, and T. Lv, “Enabling Technologies for Ultra-Reliable and Low Latency Communications: From PHY and MAC Layer Perspectives,” *IEEE Communications Surveys & Tutorials*, vol. 21, no. 3, pp. 2488–2524, 2019.

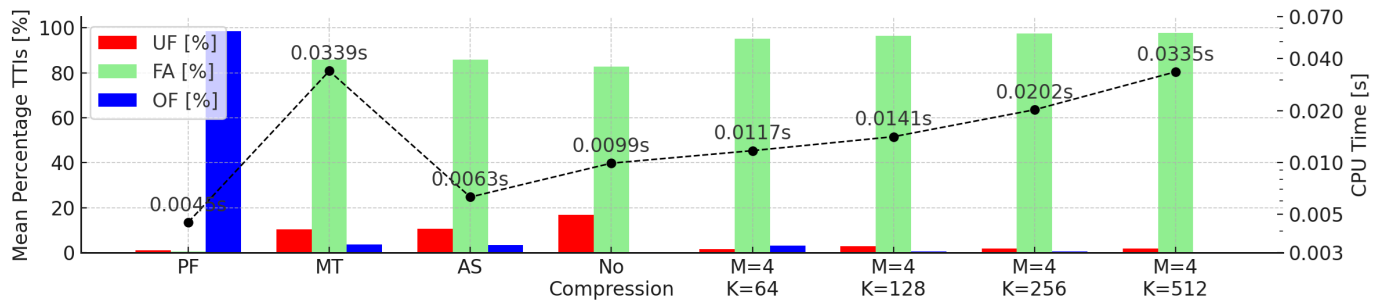


Fig. 5: Ablation Study on CQI Compression for CACLA2 and Performance Comparison With State-of-the-Art Resource Management Methods

- [3] S. A. Khan, H. Lim, and S. A. Chaudhry, "Adaptive Data Forwarding Scheme for Diverse Infotainment Services in Vehicular Named Data Networking," *IEEE Transactions on Vehicular Technology*, vol. 74, no. 5, pp. 8012–8022, 2025.
- [4] L. Wang, H. Ye, L. Liang, and G. Y. Li, "Learn to Compress CSI and Allocate Resources in Vehicular Networks," *IEEE Transactions on Communications*, vol. 68, no. 6, pp. 3640–3653, 2020.
- [5] L. Geng, H. Zhao, J. Wang, A. Kaushik, S. Yuan, and W. Feng, "Deep-Reinforcement-Learning-Based Distributed Computation Offloading in Vehicular Edge Computing Networks," *IEEE Internet of Things Journal*, vol. 10, no. 14, pp. 12416–12433, 2023.
- [6] X. Liu, H. Liu, K. Zheng, J. Liu, T. Taleb, and N. Shiratori, "AoI-Minimal Clustering, Transmission and Trajectory Co-Design for UAV-Assisted WPCNs," *IEEE Transactions on Vehicular Technology*, vol. 74, no. 1, pp. 1035–1051, 2025.
- [7] X. Liu, A. Chen, K. Zheng, K. Chi, B. Yang, and T. Taleb, "Distributed Computation Offloading for Energy Provision Minimization in WP-MEC Networks With Multiple HAPs," *IEEE Transactions on Mobile Computing*, vol. 24, no. 4, pp. 2673–2689, 2025.
- [8] B. Kim and D. Gangadharan, "Edge-Server Workload Characterization in Vehicular Computation Offloading: Semantics and Empirical Analysis," *IEEE Access*, vol. 12, pp. 89082–89097, 2024.
- [9] H. Yang, K. Zheng, L. Zhao, and L. Hanzo, "Twin-Timescale Radio Resource Management for Ultra-Reliable and Low-Latency Vehicular Networks," *IEEE Transactions on Vehicular Technology*, vol. 69, no. 1, pp. 1023–1036, 2020.
- [10] D. G. S. Pivoto, F. A. P. de Figueiredo, C. Cavdar, G. R. d. L. Tejerina, and L. L. Mendes, "A Comprehensive Survey of Machine Learning Applied to Resource Allocation in Wireless Communications," *IEEE Communications Surveys & Tutorials*, pp. 1–1, 2025.
- [11] I.-S. Comşa, *Sustainable Scheduling Policies for Radio Access Networks Based on LTE Technology*. Ph.D. dissertation, School Comput. Sci. Technol., Univ. of Bedfordshire, Luton, U.K., 2014.
- [12] P.-N. Tan, M. Steinbach, A. Karpatine, and V. Kumar, "Cluster Analysis: Basic Concepts and Algorithms," in *Introduction to Data Mining*, New York, NY :Pearson Education, Inc., vol. 7, pp. 525 – 613, 2019.
- [13] M. T. Moayyed, B. Antonescu, and S. Basagni, "Clustering Validation for mmWave Multipath Components in Outdoor Transmissions," in *2019 Wireless Days (WD)*, 2019, pp. 1–8.
- [14] K. M. Thilina, K. W. Choi, N. Saquib, and E. Hossain, "Machine Learning Techniques for Cooperative Spectrum Sensing in Cognitive Radio Networks," *IEEE Journal on Selected Areas in Communications*, vol. 31, no. 11, pp. 2209–2221, 2013.
- [15] M. S. Parwez, D. B. Rawat, and M. Garuba, "Big Data Analytics for User-Activity Analysis and User-Anomaly Detection in Mobile Wireless Networks," *IEEE Transactions on Industrial Informatics*, vol. 13, no. 4, pp. 2058–2065, 2017.
- [16] S. E. Hajri and M. Assaad, "Energy Efficiency in Cache-Enabled Small Cell Networks With Adaptive User Clustering," *IEEE Transactions on Wireless Communications*, vol. 17, no. 2, pp. 955–968, 2018.
- [17] T. Kanungo, D. M. Mount, N. S. Netanyahu, C. D. Piatko, R. Silverman, and A. Y. Wu, "A Local Search Approximation Algorithm for K-means Clustering," in *Proceedings of the Eighteenth Annual Symposium on Computational Geometry*, 2002, pp. 10 – 18.
- [18] M. Mohri, A. Rostamizadeh, and A. Talwalkar, *Foundations of Machine Learning*. The MIT Press Cambridge, Massachusetts, London, England, 2012.
- [19] F. Azmat, Y. Chen, and N. Stocks, "Analysis of Spectrum Occupancy Using Machine Learning Algorithms," *IEEE Transactions on Vehicular Technology*, vol. 65, no. 9, pp. 6853–6860, 2016.
- [20] C. Zhang, H. Zhang, J. Qiao, D. Yuan, and M. Zhang, "Deep Transfer Learning for Intelligent Cellular Traffic Prediction Based on Cross-Domain Big Data," *IEEE Journal on Selected Areas in Communications*, vol. 37, no. 6, pp. 1389–1401, 2019.
- [21] A. Albanna and H. Yousefi zadeh, "Learning-Constrained Enhancement of Cellular Networks Capacity," *IEEE Transactions on Mobile Computing*, vol. 18, no. 1, pp. 153–164, 2019.
- [22] N. Magaia and Z. Sheng, "ReFloV: A Novel Reputation Framework for Information-Centric Vehicular Applications," *IEEE Transactions on Vehicular Technology*, vol. 68, no. 2, pp. 1810–1823, 2019.
- [23] L. Li, Y. Xu, Z. Zhang, J. Yin, W. Chen, and Z. Han, "A Prediction-Based Charging Policy and Interference Mitigation Approach in the Wireless Powered Internet of Things," *IEEE Journal on Selected Areas in Communications*, vol. 37, no. 2, pp. 439–451, 2019.
- [24] S. Haykin, *Neural Networks: A Comprehensive Foundation, Second Edition*. Prentice Hall, 1999.
- [25] F. D. Calabrese, L. Wang, E. Ghadimi, G. Peters, L. Hanzo, and P. Soldati, "Learning Radio Resource Management in RANs: Framework, Opportunities, and Challenges," *IEEE Communications Magazine*, vol. 56, no. 9, pp. 138–145, 2018.
- [26] Y. Xia, L. Wu, Z. Wang, X. Zheng, and J. Jin, "Cluster-Enabled Cooperative Scheduling Based on Reinforcement Learning for High-Mobility Vehicular Networks," *IEEE Transactions on Vehicular Technology*, vol. 69, no. 11, pp. 12664–12678, 2020.
- [27] H. Ma, S. Li, E. Zhang, Z. Lv, J. Hu, and X. Wei, "Cooperative Autonomous Driving Oriented MEC-Aided 5G-V2X: Prototype System Design, Field Tests and AI-Based Optimization Tools," *IEEE Access*, vol. 8, pp. 54288–54302, 2020.
- [28] M. K. Abdel-Aziz, C. Perfecto, S. Samarakoon, M. Bennis, and W. Saad, "Vehicular Cooperative Perception Through Action Branching and Federated Reinforcement Learning," *IEEE Transactions on Communications*, vol. 70, no. 2, pp. 891–903, 2022.
- [29] H. Kim and Y. Han, "An Opportunistic Channel Quality Feedback Scheme for Proportional Fair Scheduling," *IEEE Communications Letters*, vol. 11, no. 6, pp. 501–503, 2007.
- [30] M. Cordina and C. J. Debono, "A CQI Feedback Clustering Technique for Signaling Traffic Reduction During Crowd Events in 3GPP LTE Systems," in *2017 IEEE 28th Annual International Symposium on Personal, Indoor, and Mobile Radio Communications (PIMRC)*, 2017, pp. 1–6.
- [31] T. Wang, C.-K. Wen, S. Jin, and G. Y. Li, "Deep Learning-Based CSI Feedback Approach for Time-Varying Massive MIMO Channels," *IEEE Wireless Communications Letters*, vol. 8, no. 2, pp. 416–419, 2019.
- [32] A. Chiumento, C. Desset, S. Pollin, L. Van der Perre, and R. Lauwereins, "Impact of CSI Feedback Strategies on LTE Downlink and Reinforcement Learning Solutions for Optimal Allocation," *IEEE Transactions on Vehicular Technology*, vol. 66, no. 1, pp. 550–562, 2017.
- [33] N. G. of Mobile Networks, "NGMN Radio Access Performance Evaluation Methodology," January 2008, Accessed: December, 16, 2018. [Online]. Available: https://www.ngmn.org/fileadmin/user_upload/NGMN_Radio_Access_Performance_Evaluation_Methodology.pdf.
- [34] M. Lin and J. Wawrzyn, "Improving FPGA Placement With Dynamically Adaptive Stochastic Tunneling," *IEEE Transactions on Computer-Aided Design of Integrated Circuits and Systems*, vol. 29, no. 12, pp. 1858–1869, 2010.
- [35] T. Kanungo, D. Mount, N. Netanyahu, C. Piatko, R. Silverman, and A. Wu, "An Efficient K-means Clustering Algorithm: Analysis and Implementation," in *IEEE Transactions on Pattern Analysis and Machine Intelligence*, vol. 24, no. 7, pp. 881–892, 2002.
- [36] G. Piro, L. A. Grieco, G. Boggia, F. Capozzi, and P. Camarda, "Simulating LTE Cellular Systems: An Open-Source Framework," in *IEEE Trans. on Vehicular Nets.*, vol. 60, no. 2, pp. 498 – 513, 2011.